Transverse Electrodes for Improved DNA Hybridization in Microchannels

Siddhartha Das and Suman Chakraborty
Dept. of Mechanical Engineering, Indian Institute of Technology, Kharagpur Kharagpur 721302, India

DOI 10.1002/aic.11144
Published online March 19, 2007 in Wiley InterScience (www.interscience.wiley.com).

The present study examines the modality, in which localized transverse electric fields can be successfully employed, to augment the rate of DNA hybridization at the capturing probes that are located further downstream relative to the inlet section of a rectangular microchannel. This is in accordance with an enhanced strength of convective transport that can be achieved, on account of increments in the wall zeta potential at the transverse electrode locations. In the present model, the overall convective transport, which is an implicit function of the magnitude and the location of the transverse electrical field being employed, is essentially coupled with the surface kinetics of the bare silica wall and also the kinetics that are involved in the dual mechanisms of DNA hybridization. Parameters that govern the overall transport phenomena, such as the pH of the inlet buffer, the length of the transverse electrodes, and the voltages at which these electrodes are maintained are critically examined, in an effort to obtain an optimized wall pH distribution, which in turn can ensure favorable DNA hybridization rates at the capturing probe locations. Practical constraints associated with the upper limits of the strength of the transverse electrical fields that can be employed are also critically analyzed, so as to ensure that an optimized rate of DNA hybridization can be achieved from the bio-microfluidic arrangement, without incurring any adverse effects associated with the overheating of the DNA molecules leading to their thermal denaturation. © 2007 American Institute of Chemical Engineers *AIChE J,* 53: 1086–1099, 2007

Keywords: electro-osmosis, microchannel, DNA hybridization, surface kinetics

Introduction

Research investigations on DNA hybridization in presence of microfluidic transport have attracted serious attention over recent times, primarily motivated by an ever-increasing necessity of optimizing the hybridization performance, in tune with the stringent biotechnological demands. Starting from the pioneering efforts of Chan et al.,[1] several researchers have come up with reaction-diffusion models of DNA hybridization in microfluidic channels. In this respect, the receptor–ligand model of Axelrod and Wang[2] and the dual mechanism based hybridization model of Zeng et al.[3] need special mention. Erickson et al.[4] proposed a comprehensive model of dynamic solid-phase oligonucleotide hybridization kinetics, based on an approach that accounted for both the direct hybridization from the bulk phase and hybridization after an initial nonspecific adsorption stage. Das et al.,[5] in a more recent study, have extended the earlier models to incorporate the effects of electro-osmotic transport on the DNA hybridization mechanisms. Utilization of electrokinetic body forces in such bio-microfluidic applications has primarily been motivated by the possibility of building efficient flow control devices, without involving any moving components. Irrespective of the details of the flow actuation mechanisms, it also needs to be mentioned in this context that in principle, the DNA hybridization rates could be significantly enhanced by arranging for more efficient mixing mechanisms in the associated fluidic systems. This is because of the fact that a

Correspondence concerning this article should be addressed to S. Chakraborty at suman@mech.iitkgp.ernet.in.

better mixing ensures faster reaction kinetics in reactive microfluidic systems. Micromixing augmentation mechanisms, such as the use of pulsatile flows,[6–8] serpentine channels,[9,10] creation of slanted wells at the floor of the channel,[11] presence of surface inhomogenities,[12] surface patterning,[13] inhomogeneous zeta potential[14] etc, can therefore be potentially explored to achieve faster DNA hybridization kinetics in microchannels. Such arrangements, in effect, can overcome the technological constraints associated with the stringent limitations in employing large pressure gradients and/or electric fields under practical operating conditions, leading to an optimized DNA hybridization performance, consistent with the chosen bio-microfluidic configuration.

It is well known that the axial variations in the wall zeta potential, established on account of local pH gradients, can be utilized to modulate electro-osmotic transport in microchannels to a significant extent in many of the biomicrofluidic applications.[15,16] However this effect is yet to be well exploited to obtain favorable DNA hybridization patterns. Fundamentally, localized variations in the wall zeta potential can alter the number of hydrogen ions that can be adsorbed at the channel walls, thereby altering the electrical potential distribution in the vicinity. Utilizing this basic principle, several techniques, including the popular method of isoelectric focusing,[17] have been successfully employed by the research community, for the purpose of separation of analytes on the basis of their respective isoelectric points, as a consequence of the development of transverse potential gradients established across a pair of surface electrodes.[18] In a pioneering study, Molloy and Leighton demonstrated the effectiveness of employing transverse electric fields to perform binary oscillatory cross flow electrophoresis.[19] Amongst the other important studies in related applications, the investigations of Chan and Chauhan on the employment of transverse electrodes for performing cyclic EFFF[20] and the use of EFFF for size-based separation of DNA molecules[21] also worth special mention. However, in case of DNA transport, systematic theoretical guidelines are yet to be put forward, so as to exploit a deliberate generation of pH gradients through a designed configuration of transverse electrode pairs, in an effort to augment the rate of hybridization in electrokinetically driven microfluidic systems. Such attempts, in reality, can bear significant consequences, leading towards a maximization of DNA hybridization rates, within the constraints of a maximum permissible potential gradient that can be imposed on the microfluidic system.

The aim of the present work is to theoretically demonstrate how a strong local pH gradient, obtained by employing a pair of transverse electrodes, can be effectively utilized to achieve a faster rate of DNA hybridization in a microchannel. The conceptual system design is exercised by avoiding any direct interference between the positioning of transverse electrodes and surface DNA probes on the microchannel walls, so as to provide a technological feasibility to the entire arrangement. In other words, the DNA probes are considered to be located sufficiently downstream or upstream to the transverse electrodes. The model, in essence, couples the surface kinetics, as modified by the presence of the transverse electrodes, with the bulk transport of momentum, heat, ionic species, and DNA macromolecules, from the fundamental physico-chemical principles. Based on the mathematical model, simulation experiments are undertaken, so as to depict the influence of the significant system parameters, such as the pH of the buffer solution at the inlet, voltages at the transverse electrodes, and the electrode dimensions, on the resultant DNA hybridization rates. An upper limit of the extent to which the transverse electric fields can be exploited to augment the rate of DNA hybridization is also established, so as to constrain the associated Joule heating effects within permissible standards, to avoid a further thermal denaturation of the double stranded (hybridized) DNA macromolecules. To establish the afore-mentioned basic principles from a fundamental mathematical perspective, a relatively simple configuration is chosen, which assumes only a pair of capturing DNA probes, positioned symmetrically on both sides of a central electrode located on the bottom wall of a parallel plate microchannel, with another electrode of the same length being located on the upper wall, at the same axial location. For more involved designs, this arrangement can be considered as a repeating monoblock, the number of which depends on the desired complexity of the system chosen, in accordance with the DNA hybridization rates sought. Underlying principles of this simple model, therefore, can be conveniently extended to obtain favorable hybridization patterns in more complicated situations as well, in which there are provisions to employ larger numbers of DNA probes and matching transverse electrode pairs in the microfluidic system.

Mathematical Modeling

We consider electro-osmotic transport of an ionic solution of water through a parallel plate microchannel, made of bare silica, of length L_0, height H, and width w, with $w \gg H$ and a subsequent hybridization of transported ss-DNA molecules with their complementary pairs that are immobilized at the two different probe locations along the bottom wall of the channel. A potential gradient is applied along the axis of the channel, which provides the necessary driving force for electrokinetic transport. The magnitude of this potential gradient is ascertained by assigning a specified potential, ϕ_0, (given in Table 1) at the channel inlet and a zero potential at the channel exit. Typically, ϕ_0 is so chosen that the axial electric field becomes of the order of 10^5 V/m, as a common technological practice. In addition to this axial field, a local transverse electric field is applied by maintaining two transverse electrodes at different voltages, the transverse field being confined over a limited portion of the channel length only. The magnitude of this transverse field is varied in the range of 10^5–10^6 V/m, by altering the cross-electrode potentials. The effects of variations of the transverse potential gradients on the DNA hybridization are illustrated later in this article. We assume that in the hybridization channel no bubbles are being generated due to the electrochemical reaction on these transverse electrodes We consider the two DNA hybridization probes to be located at equal distances on either side of the transverse electrode. The entire arrangement is schematically represented in Figure 1. In effect, the DNA molecules are transported by the combined actions of the electro-osmotic and the electrophoretic migration mechanisms in the axial as well as in the transverse directions. Because of a negative charge on the DNA molecules, the electrophoretic influences on those effectively oppose their

Table 1. Summary of Boundary Conditions

Governing Equation	Inlet ($x = 0$)	Outlet ($x = L_0$)	Bottom Wall ($y = 0$)	Top Wall ($y = H$)
Poisson-Boltzmann eq. (Eq. 5)	$\psi = 0$	$\frac{\partial \psi}{\partial x} = 0$	$\psi = \zeta$ (zeta Potential)	$\psi = \zeta$ (zeta Potential)
Fluid flow eqs. (eq. 1–3)	$\mathrm{u} = \mathrm{u}_{\mathrm{in}}$	$\frac{\partial u}{\partial x} = 0$ $v = 0$	$\mathrm{u} = 0$ $v = 0$	$\mathrm{u} = 0$ $v = 0$
Energy conservation eq. (Eq. 13)	$T = T_\infty$	$\frac{\partial T}{\partial x} = 0$	$-k\frac{\partial T}{\partial y} = q''$	$-k\frac{\partial T}{\partial y} = q''$
Conservation equation for concentration of the cations (Eq. 8)	$c_{\mathrm{H}^+} = (c_{\mathrm{H}^+})_{\mathrm{inter}}$ $c_{\mathrm{M}^{n+}} = (c_{\mathrm{M}^{n+}})_{\mathrm{inter}}$	$\frac{\partial c_{\mathrm{H}^+}}{\partial x} = 0$ $\frac{\partial c_{\mathrm{M}^{n+}}}{\partial x} = 0$	$c_{\mathrm{H}^+} = c_{\mathrm{H}^+}^{\mathrm{film}} \exp\left(-\frac{e\psi}{k_{\mathrm{B}}T}\right)$ $c_{\mathrm{M}^{n+}} = c_{\mathrm{M}^{n+}}^{\mathrm{film}} \exp\left(-\frac{ne\psi}{k_{\mathrm{B}}T}\right)$	$c_{\mathrm{H}^+} = c_{\mathrm{H}^+}^{\mathrm{film}} \exp\left(-\frac{e\psi}{k_{\mathrm{B}}T}\right)$ $c_{\mathrm{M}^{n+}} = c_{\mathrm{M}^{n+}}^{\mathrm{film}} \exp\left(-\frac{ne\psi}{k_{\mathrm{B}}T}\right)$
Conservation eq. for concentration of anions (Eq. 8)	$c_{\mathrm{OH}^-} = (c_{\mathrm{OH}^-})_{\mathrm{inlet}}$ $c_{\mathrm{X}^{n-}} = (c_{\mathrm{X}^{n-}})_{\mathrm{inlet}}$	$\frac{\partial c_{\mathrm{OH}^-}}{\partial x} = 0$ $\frac{\partial c_{\mathrm{X}^{n-}}}{\partial x} = 0$	$c_{\mathrm{OH}^-} = c_{\mathrm{OH}^-}^{\mathrm{film}} \exp\left(\frac{e\psi}{k_{\mathrm{B}}T}\right)$ $c_{\mathrm{X}^{n-}} = c_{\mathrm{X}^{n-}}^{\mathrm{film}} \exp\left(\frac{ne\psi}{k_{\mathrm{B}}T}\right)$	$c_{\mathrm{OH}^-} = c_{\mathrm{OH}^-}^{\mathrm{film}} \exp\left(\frac{e\psi}{k_{\mathrm{B}}T}\right)$ $c_{\mathrm{X}^{n-}} = c_{\mathrm{X}^{n-}}^{\mathrm{film}} \exp\left(\frac{ne\psi}{k_{\mathrm{B}}T}\right)$
Conservation eq. for DNA concentration (Eq. 8)	$c_{\mathrm{DNA}} = (c_{\mathrm{DNA}})_{\mathrm{inlet}}$	$\frac{\partial c_{\mathrm{DNA}}}{\partial x} = 0$	$\frac{\partial c_{\mathrm{DNA}}}{\partial y} = 0$	$\frac{\partial c_{\mathrm{DNA}}}{\partial y} = 0$

electro-osmotic migration. However, the electro-osmotic mobility of the DNA molecules being greater than their electrophoretic mobility, this retarding effect gets effectively overweighed, and the DNA molecules move in the direction of electro-osmotic transport. This aspect is further elucidated through the numerical simulation predictions, as discussed later.

Convection–diffusion transport equations

The governing transport equations, under these circumstances, can be described as follows.

Continuity Equation.

$$\frac{\partial \rho}{\partial t} + \nabla \bullet (\rho \vec{V}) = 0 \tag{1}$$

X-Momentum Equation.

$$\frac{\partial}{\partial t}(\rho u) + \nabla \bullet (\rho \vec{V} u) = -\frac{\partial p}{\partial x} + \nabla \bullet (\mu \nabla u) - \rho_e \left(\frac{\partial \phi}{\partial x} + \frac{\partial \psi}{\partial x}\right) \tag{2}$$

where ρ_e is the net electric charge density, ϕ is the potential distribution due to an externally imposed electric field and ψ is the surface potential distribution.

Y-Momentum Equation.

$$\frac{\partial}{\partial t}(\rho v) + \nabla \bullet (\rho \vec{V} v) = -\frac{\partial p}{\partial y} + \nabla \bullet (\mu \nabla v) - \rho_e \left(\frac{\partial \phi}{\partial y} + \frac{\partial \psi}{\partial y}\right) \tag{3}$$

In both Eqs. 2 and 3, the dynamic viscosity, μ, is a function of temperature, given as[22]

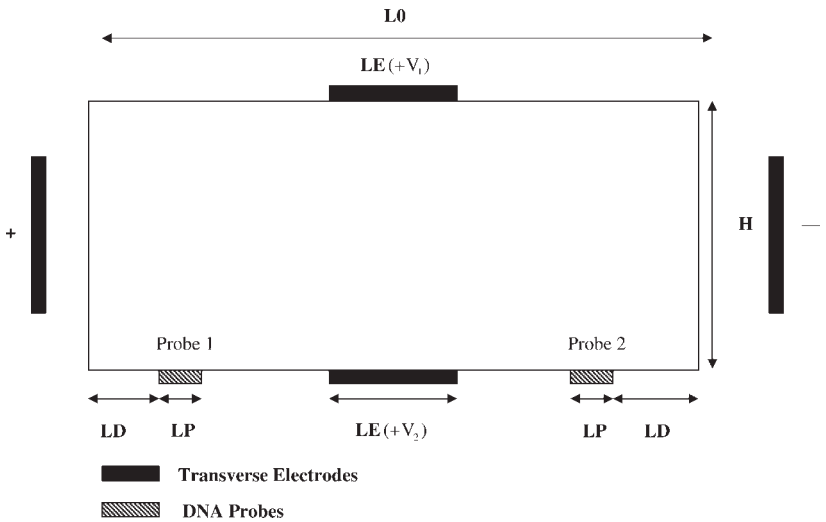

Figure 1. The flow configuration.

$$\mu = 2.761 \times 10^{-6} \exp\left(\frac{1713}{T}\right) \tag{4}$$

where T is in K and μ is in Pa s.

Distribution of the net electric charge density, ρ_e, appearing in the momentum conservation equations, can be ascertained by solving the Poisson–Boltzmann equation for surface potential distribution as

$$\nabla \bullet (\varepsilon \nabla \psi) = -\frac{\rho_e}{\varepsilon_0} \tag{5}$$

where ψ denotes the electric double layer (EDL) potential, ε_0 is the permittivity of free space, and ε is the dielectric constant of the electrolyte, which is a function of temperature, given as[22]

$$\varepsilon = 305.7 \exp\left(-\frac{T}{219}\right) \tag{6}$$

where T is in K. In Eq. 5, ρ_e, is described as

$$\rho_e = 10^3 N_a \, e \sum_{i=1}^{N} z_i c_i \tag{7}$$

Here z_i and c_i are the valency and the concentration of the i^{th} ionic species, respectively, N_a is the Avogadro number and N is the total number of ionic species in the solution. The concentration of the i^{th} ionic species is governed by the species-conservation equation, given by

$$\frac{\partial(\rho c_i)}{\partial t} + \nabla \bullet (\rho \vec{V} c_i) = \nabla \bullet (\rho D_i \nabla c_i) + \nabla \bullet (\rho \mu_{ep,i} c_i \nabla \phi) + \rho R_i \tag{8}$$

In Eq. 8, R_i is the term responsible for any reaction that the ionic species may undergo in the solution. The term $\mu_{ep,i}$ represents the electrophoretic mobility of the i^{th} species, which depends on the nature of species being transported. For the ss-DNA molecules, $\mu_{ep,i}$ is given by[23]

$$\mu_{ep,i} = [f(\kappa a_i)/(1 + \kappa a_i)] e z_i \omega_{H,i}, \tag{8a}$$

In Eq. 8a, κ is the inverse of the Debye length, z_i is the valence of the i^{th} type of the ss-DNA molecule (which can be obtained through Eq. 11, as described subsequently), a_i is its Stokes radius, $\omega_{H,i}$ is its hydrodynamic mobility (which can be expressed as $\omega_{H,i} = \frac{1}{6\pi\mu a_i}$ and $f(\kappa a_i)$ is the Henry's f-function. However, for the other ionic species, the electrophoretic mobility can be more simply expressed as

$$\mu_{ep,i} = e z_i \omega_{H,i} \tag{8b}$$

In the present model, we consider simple ionic species in the solution, with the following constituents: H^+, OH^-, M^{n+}, X^{n-}, where X^{n-} is the anion corresponding to the added metallic cation, M^{n+}. The other kind of ionic species that might be expected to be present in the solution will include traces of some phosphates or sulfates, which are routinely added to alter certain properties of the solution, such as its conductivity. However, these components are present in much smaller amounts when compared with M^{n+} or X^{n-}, and hence, the effects of their presence are neglected in the present study. We also consider that only a single type of ss-DNA molecules is being transported. While considering transport of the ss-DNA species, the diffusion coefficient D_i, appearing in Eq. 8 represents a generalized diffusion coefficient, which is the liquid phase diffusion coefficient (D_3) in the bulk fluid and surface phase diffusion coefficient (D_2) at the nonspecific adsorption sites (It can be noted here that DNA hybridization can take place directly from the bulk phase (3D hybridization) or along the wall surface (2D hybridization) after an initial nonspecific adsorption step.). By borrowing analogy from diffusion transport of polymeric chains, the diffusion coefficients for DNA molecules can be expressed as the functions of the size and concentration of the ss-DNA molecules, along with the ionic strength of the solution. Typically, one can employ certain well-established scaling relationship for this purpose, for example[24]

$$\frac{D_i}{D_{i,0}} = \exp\left(-\alpha c^{\nu} R^{\delta}\right) \tag{9}$$

where D_i is the effective diffusion coefficient of a DNA macromolecule of radius R and concentration c, and $D_{i,0}$ is the corresponding diffusion coefficient for $c = 0$. Experiments on a wide range of polymer systems, both biological and synthetic,[25–27] have shown that such scaling laws can adequately describe the diffusion of a polymer over a wide range of solution concentrations. From a series of investigations, it has been revealed that the parameter v, as appearing in Eq. 9, typically falls in the range of 0.5–1.0, with the lower and the upper limits signifying the relative contributions of hydrodynamic and direct interactions, respectively. The parameter δ varies from 0 to 1, depending upon the polymer system. The parameter α is a function of the ionic strength of the solution given as $\alpha \sim I^{\beta}$, where I is the ionic strength and β is a function of the nature of the polymer solution. In the present study, we estimate the earlier parameters by considering a total of 10 nucleotide units of ss-DNA molecules with a hydrodynamic radius of around 1 nm, by referring to the scaling estimates developed by Dwyer and Bloomfield.[24] Diffusivities of the other ionic species, however, can be estimated in a more straightforward manner as

$$D_i = \omega_{H,i} k_B T \tag{9a}$$

It also needs to be noted here that an accurate solution of the species conservation equation (Eq. 8) not only requires a physically-consistent specification of the diffusion coefficients, but also necessitates a correct specification of the electro-osmotic mobilities of the ionic species, which in turn depend on the respective charges of the ionic species being transported. For that purpose, it can be noted that unlike the simple ionic species, charges of the ss-DNA molecules do not remain constant for all values of the buffer pH. A quantitative description of the electrostatic characteristics of a ss-DNA molecule, as a function of the buffer pH, can be derived from the ionization of the phosphodiester linkages (resulting in one negative charge per nucleotide) and also from ionization of bases (making the charge on the DNA base-dependent) in an aqueous solution. A phosphodiester is

a strong acid whose pK is around 1. Nucleotides which make up the DNA molecules can be of four types differing only in the nitrogenous base: Adenine, Thymine, Cytosine and Guanine. Adenine (A), and Cytosine (C) bases can be found as neutral or positive forms, whereas thymine (T) is neutral or negative, and guanine (G) can exist in all the three states.[28] The ionization of these bases can be represented as

$$\textbf{Adenine}: [AH^+] \overset{K_A}{\longleftrightarrow} [A] + [H^+] \qquad K_A = 10^{-3.5} \tag{10a}$$

$$\textbf{Cytosine}: [CH^+] \overset{K_C}{\longleftrightarrow} [C] + [H^+] \qquad K_C = 10^{-4.2} \tag{10b}$$

$$\textbf{Thymine}: [TH] \overset{K_T}{\longleftrightarrow} [T^-] + [H^+] \qquad K_T = 10^{-9.2} \tag{10c}$$

$$\textbf{Guanine}: [GH_2^+] \overset{K_{G_1}}{\longleftrightarrow} [GH] + [H^+] \qquad K_{G_1} = 10^{-2.1} \tag{10d}$$

$$[GH] \overset{K_{G_2}}{\longleftrightarrow} [G^-] + [H^+] \qquad K_{G_2} = 10^{-9.2} \tag{10e}$$

Now, assuming the probability of presence of each base type (A, T, C, G) to be 25% per nucleotide, the average net charge per nucleotide, C/N_{nu}, may be estimated as[28]

$$C/N_{nu} \approx -\frac{1}{1+[H^+]/K_{ph}} + 0.25\frac{1}{1+K_A/[H^+]} + 0.25\frac{1}{1+K_C/[H^+]} - 0.25\frac{1}{1+[H^+]/K_T} + 0.25\frac{[H^+]^2 - K_{G1}K_{G2}}{K_{G1}K_{G2} - K_{G1}[H^+] + [H^+]^2} \tag{11}$$

where K_{ph} ($=10^{-1}$) corresponds to the ionization of the phosphodiester groups. The valency term z_i appearing in the species conservation equation for the ss-DNA molecule is identical to the average net charge per nucleotide C/N_{nu} and is thus given by Eq. (11).

It can be noted here that an accurate modeling of the second term in the right hand side of Eq. 8 not only demands a consistent description of the electro-osmotic mobilities of the constituents, but also requires a specification of the distribution of the potential field, ϕ, which can be obtained by considering the charge conservation in the liquid, in accordance with the requirement of $\nabla I = 0$. This finally leads to a differential equation governing the distribution of ϕ as

$$\nabla \bullet (\sigma \nabla \phi) = -\nabla \vec{i}^{\,D} \tag{12}$$

where i^D is the diffusion current density and σ is the electrical conductivity, given as[23]

$$\sigma = 10^3 N_a e^2 \left[\sum_{i=1}^{M_p} \frac{f(\kappa a_i)}{1+\kappa a_i} z_i^2 \omega_{H,i} c_i + \sum_{i=M_p+1}^{N-2} z_i^2 \omega_{H,i} c_i + \omega_{H,H^+} c_{H^+} + \omega_{H,OH^-} \frac{K_w}{c_{H^+}} \right] \tag{12a}$$

In Eq. 12a, K_w is the dissociation constant for water. In the earlier formulation, we assume that in totality there are M_P types of different ss-DNA molecules in the solution, and (N-2-M_P) types of ionic species, other than the H^+ and OH^- ions. For the present model, $M_P = 1$ and $N = 5$.

Thermal energy conservation equation

Since various physico-chemical characteristics pertinent to the present model are very much temperature sensitive, a solution of the energy equation also turns out to be necessary. The earlier equation can be cast in the following general form:

$$\frac{\partial}{\partial t}(\rho C_P T) + \nabla \bullet (\rho C_P \vec{V} T) = \nabla \bullet (k \nabla T) + \varphi + \dot{q} \tag{13}$$

where k is the thermal conductivity of the electrolyte solution, which is a function of temperature, given as[22]

$$k = 0.6 + 2.5 \times 10^{-5} T \tag{14}$$

where T is in K and k is in W/m^2 K. In Eq. 13, φ is the volumetric heat generation due to viscous dissipation, given as

$$\varphi = 2\mu \left[\left(\frac{\partial u}{\partial x}\right)^2 + \left(\frac{\partial v}{\partial y}\right)^2 \right] + \mu \left(\frac{\partial u}{\partial y} + \frac{\partial v}{\partial y}\right)^2 \tag{15}$$

Further, $\dot{q}$ is the volumetric heat generation due to Joule effects, which, according to Ohm's law, can be given as

$$\dot{q} = \frac{I^2}{\sigma} \tag{16}$$

where I is the electrical current density and σ is the electrical conductivity. It can be noted here that the electrical current density includes two specific contributions, one due to the applied electric field imposed on the conducting solution ($\sigma\vec{E}$), and the other due to the net charge density moving with the fluid flow ($\rho_e \vec{V}$). Therefore, the electrical current density, $\vec{I}$, can expressed as

$$\vec{I} = \rho_e \vec{V} + \sigma \vec{E} \tag{17}$$

Using Eqs. 16 and 17, one can obtain an expression for $\dot{q}$ as

$$\dot{q} = \frac{(\rho_e \vec{V} + \sigma \vec{E}) \bullet (\rho_e \vec{V} + \sigma \vec{E})}{\sigma} \tag{18}$$

Coupling of transport modeling with DNA hybridization kinetics

The model of species (DNA) transport adopted here is based on two basic mechanisms of hybridization, namely, direct (specific) hybridization from the bulk phase to the surface-bound probes, and by indirect (nonspecific) hybridization, in which the target is initially nonspecifically adsorbed on the surface and then diffuses along the surface before reaching an available target probe molecule. Details of these

mechanisms are outlined in Erickson et al.,[4] and are not repeated here for the sake of brevity. However, a summary of the pertinent formulation is presented here, for the sake of completeness. Effectively, we implement the hybridization boundary conditions at the bottom wall by invoking the generic source term, R_i, appearing in Eq. 8 such that, for the bulk phase, $R_i = 0$, and for the reactive bottom wall (where the capturing probes are attached)

$$R_i = -\left(\frac{\partial c_{2,\mathrm{s}}}{\partial t} + \frac{\partial c_{2,\mathrm{ns}}}{\partial}\right) \tag{19}$$

where, $c_{2,\mathrm{s}}$ and $c_{2,\mathrm{ns}}$ are the surface-phase concentration of specifically and nonspecifically adsorbed target molecules, respectively. Along the nonreacting surfaces, however, $R_i = 0$. The terms appearing in Eq. 19 can further be expressed as a set of coupled two-dimensional kinetic equations as

$$\frac{\partial c_{2,\mathrm{s}}}{\partial t} = [k_3^1 c_{3,\mathrm{m}}(c_{2,\mathrm{s,max}} - c_{2,\mathrm{s}}) - k_3^{-1} c_{2,\mathrm{s}}] + [k_2^1 c_{2,\mathrm{ns}}(c_{2,\mathrm{s,max}} - c_{2,\mathrm{s}}) - k_2^{-1} c_{2,\mathrm{s}}] \tag{20}$$

and

$$\frac{\partial c_{2,\mathrm{ns}}}{\partial t} = [k_\mathrm{a} c_{3,\mathrm{m}}(c_{2,\mathrm{ns,max}} - c_{2,\mathrm{ns}}) - k_\mathrm{d} c_{2,\mathrm{ns}}] - [k_2^1 c_{2,\mathrm{ns}}(c_{2,\mathrm{s,max}} - c_{2,\mathrm{s}}) - k_2^{-1} c_{2,\mathrm{s}}] \tag{21}$$

where, $c_{2,\mathrm{s,max}}$ is the maximum concentration of the hybridized targets (equivalent to the local concentration of the surface bound probes available for hybridization), $c_{2,\mathrm{ns,max}}$ is the maximum concentration of the nonspecifically adsorbed molecules, $c_{3,\mathrm{m}}$ is the bulk-phase concentration of the targets in surface film, k_3^1 is the kinetic association constant for direct hybridization (from solution phase), k_3^{-1} is the kinetic dissociation constant for direct hybridization (from solution phase), k_2^1 is the kinetic association constant for indirect hybridization of the nonspecifically adsorbed targets (from surface phase), k_2^{-1} is the kinetic dissociation constant for indirect hybridization of the nonspecifically adsorbed targets (from surface phase), k_a is the kinetic association constant for nonspecific adsorption of the targets to the surface, and k_d is the kinetic dissociation constant for nonspecific adsorption of the targets to the surface. It is to be noted here that the values of k_2^{-1} and k_3^{-1} may differ from one another, since they denote dissociation constants from two different phases, i.e., the surface and the solution phases, respectively. Physically, Eq. 20 describes that the rate of change in surface concentration of hybridized species is a combination of the rate of change of targets getting hybridized directly from the bulk phase and the rate of targets getting hybridized after an initial nonspecific adsorption. Equation 21 implies that the rate of change in surface concentration of nonspecifically adsorbed targets is increased by the rate of adsorption from the bulk phase, but is decreased by the rate at which the nonspecifically adsorbed targets become hybridized. For detailed calculation of the kinetic constants appearing in Eqs. 20 and 21, Erickson et al.[4] can be referred to.

The boundary conditions consistent with various conservation equations described as earlier are summarized in Table 1.

Dependence of zeta potential on the surface kinetics

At the surface of the bare silica walls, the following reactions take place.

(1)

$$\mathrm{SiOH} \overset{K_1}{\longleftrightarrow} \mathrm{SiO^-} + \mathrm{H^+}, \tag{22}$$

where K_1 is the equilibrium constant for the earlier reaction, given as[28]

$$K_1 = \frac{[\mathrm{SiO^-}][\mathrm{H^+}]}{[\mathrm{SiOH}]} = 10^{-6} \tag{22a}$$

(2)

$$\mathrm{SiOH_2^+} \overset{K}{\longleftrightarrow} \mathrm{SiO^-} + 2\mathrm{H^+} \tag{23}$$

where K is the equilibrium constant for the earlier reaction, given as[28]

$$K = \frac{[\mathrm{SiO^-}][\mathrm{H^+}]^2}{[\mathrm{SiOH_2^+}]} = 10^{-2\mathrm{pzc}} \tag{23a}$$

Here, 'pzc' or the point of zero charge, which is the pH at which the surface density of the positive charges is equal to the surface density of the negative charges.[29] A standard practice for measuring the pzc for a given surface is to calculate the pH of a water drop at which the drop makes the largest wetting angle with the concerned surface.[28] A typical experimentally measured value[29,30] for pzc for a bare silica surface is 3, which gives $K = 10^{-6}$.

(3)

$$\mathrm{SiOH_2^+} \overset{K_2}{\longleftrightarrow} \mathrm{SiOH} + \mathrm{H^+} \tag{24}$$

where K_2 is the equilibrium constant for the earlier reaction, given as[28]

$$K_2 = \frac{[\mathrm{SiOH}][\mathrm{H^+}]}{[\mathrm{SiOH_2^+}]} = \frac{K}{K_1} = 1 \tag{24a}$$

(4) Like the other ionic species, the metallic ions present in the solution also give rise to a certain chemical reaction, as[31]

$$\mathrm{M}^{n+} + \mathrm{SiO^-} \overset{K_\mathrm{M}}{\longleftrightarrow} \mathrm{M}^{n+}\mathrm{SiO^-} \tag{25}$$

where K_M is the equilibrium constant for the earlier reaction, given as

$$K_\mathrm{M} = \frac{[\mathrm{M}^{n+}\mathrm{SiO^-}]}{[\mathrm{M}^{n+}][\mathrm{SiO^-}]} \tag{25a}$$

The value of K_M depends on the specific nature of the metallic ion. Higher the value of K_M, greater is the protonation of free silanol groups by these cations, and larger is the lowering of the zeta potential and the consequent electro-osmotic force (EOF). It needs to be noted here that although the metallic cations protonate the silanol group and thereby reduce the wall zeta potential, a presence of excess of such ions in the bulk provides the necessary driving force for the electrokinetic flow to take place. Accordingly, the presence of such

metallic ions is virtually indispensable for an efficient convective transport to take place in the buffer solution.

For an effective estimation of the concentration of the SiO^- group appearing in the afore-mentioned reactions, we first note that the surface site density, γ, can be given as

$$\gamma = N_A([SiO^-] + [SiOH] + [SiOH_2^+] + [M^{n+}SiO^-]) \quad (26)$$

where N_A is the Avogadro number. A typical value of γ for glass walls is around 4.5 sites/nm^2.[28] Combining Eqs. 22a, 23a, and 24a, along with Eq. 26, we get

$$[SiO^-] = \frac{\gamma}{N_A\left(1 + \frac{[H^+]}{K_1} + \frac{[H^+]^2}{K_1K_2} + K_M[M^{n+}]\right)} \quad (27)$$

Again, the surface charge per unit area is given as

$$\sigma_{Si} = N_A\ e([SiO^-] - [SiOH_2^+]) \quad (28)$$

(where e is the electronic charge), which can be expressed (using Eqs. 22a, 23a, and 24a) as

$$\sigma_{Si} = N_A\ e[SiO^-]\left(1 - \frac{[H^+]^2}{K_1K_2}\right) \quad (29)$$

Combining Eqs. 27 and 29, we get

$$\sigma_{Si} = \gamma\ e\left(\frac{1 - \frac{[H^+]^2}{K_1K_2}}{1 + \frac{[H^+]}{K_1} + \frac{[H^+]^2}{K_1K_2} + K_M[M^{n+}]}\right) \quad (30)$$

The net charge density, σ_{total}, which can be considered approximately same as σ_{Si}, determines the effective zeta potential as[32]

$$\zeta = \frac{2k_BT}{e}\ \sin h^{-1}\left(\sigma_{Si}\left[\frac{500\pi}{\varepsilon\varepsilon_0RT([H^+]_{Surface} + [M^{n+}]_{Surface})}\right]^{1/2}\right) \quad (31)$$

The parameters $[H^+]_{Surface}$ and $[M^{n+}]_{Surface}$, as appearing in Eq. 31, can be described through Boltzmann partitioning as[31]

$$[H^+]_{Surface} = [H^+]_{Film}\ exp\left(-\frac{e\psi}{k_BT}\right) \quad (32)$$

$$[M^{n+}]_{Surface} = [M^{n+}]_{Film}\ exp\left(-\frac{ne\psi}{k_BT}\right) \quad (33)$$

where $[H^+]_{Film}$ and $[M^{n+}]_{Film}$ are the bulk hydrogen ion and metallic ion concentrations, respectively, in a thin film adjacent to the channel surface. Eqs. 32 and 33, in effect, suffice as the necessary boundary conditions at the channel walls for the species conservation equations for the hydrogen and the metallic ions, respectively.

Effect of transverse electrodes on the overall transport phenomena

Apart from creating a local body force along the *y*-direction, the localized electrical potential gradient produced by the transverse electrodes also induces a 'field effect,' which modifies the local wall zeta potential. For a quantitative assessment of the same, the transverse electrodes can be assumed to constitute a parallel plate capacitor, which is completely filled with a dielectric material. Therefore, considering the electric field between the parallel plates, a Gaussian surface can be imagined around the interface of the dielectric and each plate. Consequently, when Gauss' law is applied, the total charge enclosed by the Gaussian surface includes both the free and the induced charges, which eventually affects the surface zeta potential.[33] This effect is known as the 'field effect,' and the resultant zeta potential is given by[33]

$$\zeta_{field\ effect} = V_T\frac{C_T}{C_{Diffuse}} \quad (34)$$

where V_T is the potential of the nearest transverse electrode and C_T is the total capacitance of the system. In Eq. 34, $C_{Diffuse}$ is the capacitance of the diffused EDL formed at the wall, which, for a unit channel width can be estimated as[33]

$$C_{Diffuse} = 7.23 \times 10^{-3}\ \cos h[(19.46\ V^{-1})\zeta]L_0 \quad (34a)$$

with ζ the wall zeta potential, L_0 is the channel length (in centimeters), and $C_{Diffuse}$ is given in the units of Faraday. Assuming the capacitance of the diffuse layer, $C_{Diffuse}$, and the capacitance of the silica channel walls, C_{wall} ($C_{wall} = \frac{\varepsilon_{silica}\ L_0}{t_{wall}}$, where ε_{silica} is the permittivity of silica and t_{wall} is the thickness of the silica channel walls, width of the channel being taken as unity) to be in series, we can obtain an expression governing the net capacitance, C_T, as

$$\frac{1}{C_T} = \frac{1}{C_{Diffuse}} + \frac{1}{C_{wall}} \quad (35)$$

Substituting the earlier expression for C_T in Eq. 34, an estimation of the local $\zeta_{field\ effect}$ can be obtained, which, physically is the zeta potential that is induced over and above the nominal value of wall zeta potential, due to an ionization of the silica wall surface and the resultant charge distribution within the EDL. Accordingly, the overall zeta potential at the location of transverse electrodes is given as

$$\zeta_{overall} = \zeta_{wall} + \zeta_{field\ effect} \quad (36)$$

Effectively, it can be inferred from Eq. 36 that an axial gradient of the zeta potential (and a consequent variation of the local pH field) is induced along the channel walls, because of a selective placement of the transverse electrodes on the same. Such a nonuniform zeta potential, in turn, ensures a nonuniform body force at different channel cross-sections, resulting in dissimilar flow patterns at different axial locations of the channel.[34] In general, it is expected that an augmented rate of electro-osmotic transport, on account of enhanced zeta potential values at the transverse electrode locations, may be responsible for an augmented rate of DNA hybridization at the probe locations in further downstream sections, a direct quantification of which happens to be the central focus of attention behind this study.

Table 2. Simulation Data

Parameter	Value
L_0	1.0×10^{-2} m
L_P	1.0×10^{-4} m
L_D	2.0×10^{-3} m
H	50×10^{-6} m
ε_0	8.854×10^{-12} (C/V_M)
e	1.6×10^{-19} C
ϕ_0	5000 V
$u_{initial}$	2.0 m/s
a_{DNA} (Stokes radius for DNA)	1 nm
K_W	10^{-14}
T_∞	300 K
ρ	998 kg/m^3
k_B	1.38×10^{-23} J/K
Z_{K^+}	+1
Z_{Cl^-}	−1
a_{K^+} (radius of potassium ion)	1.33 Å
a_{Cl^-} (radius of chlorine ion)	1.67 Å
q''	−10 W/m^2
$(C_{DNA})_{inlet}$	1.0×10^{-6} M
$C_{3,m}$	1.9×10^{-7} M
$C_{2,s,max}$	2.0×10^{-7}/mol/m^2
$C_{2,ns,max}$	1.98×10^{-7}/mol/m^2
$k_{3^{-1}}$	1×10^6 (1/Ms)
$k_{3^{-1}}$	0.49 (1/s)
k_2^1	1×10^6 m/Ms
k_2^{-1}	0.51 (1/s)
k_a	9×10^3 (1/Ms)
k_d	0.3 (1/s)
$D_{3,0}$	1.3×10^{-10} m^2/s
$D_{2,0}$	5.0×10^{-13} m^2/s
t_{wall}	20×10^{-6} m
ε_{Silica} (Dielectric constant for silica)	4.3

Results and Discussions

To obtain a quantitative prediction from the present model, we investigate the case of electro-osmotic flow of a KCl ionic solution, with an inlet buffer pH of 4 and a uniform inlet velocity profile (u_{in}). The transverse electrodes are each taken to be of length $L_0/5$, and are maintained at +15 V (top electrode) and +20 V (bottom electrode). The other relevant problem data are listed in Table 2.

Figure 2a gives the variation of the wall pH (at the bottom wall) along the channel length, for the afore-mentioned case. From the plot it is evident that there is a significant deviation of the wall pH when compared with the inlet buffer pH, over that section of the channel length where the transverse electrodes are placed. Such significant changes in the pH cannot be induced by means of a mere convective transport. This can be attributed to the short-ranged electrostatic forces of attraction, by which the positively charged hydrogen ions remain bound to the negatively charged silica ions of the wall, which effectively happen to be too strong to be disrupted by the flow field alone. However, the presence of localized transverse electric fields, as in the present case, modifies the H^+ ion distribution within the Stern layer, thereby altering the wall zeta potential in the vicinity. This is clearly manifested by the variation of wall zeta potential along the channel length, which is depicted in Figure 2b, for the bottom wall. This variation in the local zeta potential bears a significant consequence in modifying the relative ionic distribution at the top and the bottom walls of the channel, which effectively govern the local velocity variations in vicinity of the transverse electrodes. At the channel sections where there are no transverse electrodes, the identical values of the zeta potential at the two walls effectively ensure that the velocity profile has a plug-like shape, which is typical to any fully developed electro-osmotic flow. However, for the sections containing the transverse electrodes, the wall zeta potential does not remain the same for the top and the bottom walls (Figure 3), because of the fact that the top and bottom electrodes are maintained at different voltages. Unequal voltages at the top and the bottom electrodes ensure that the 'field effect' attenuates the zeta potential to different extents at the two walls. The consequence of this becomes evident in the variations of the ionic concentration distributions at the top and the bottom channel walls (Figure 4). At the locations where there are no electrodes, the distribution of a particular type of ion (either anion or cation) remains identical at both the top and the bottom walls, leading to the typical plug-like and symmetrically-shaped electro-osmotic velocity profiles (Figure 5). However, at the channel sections

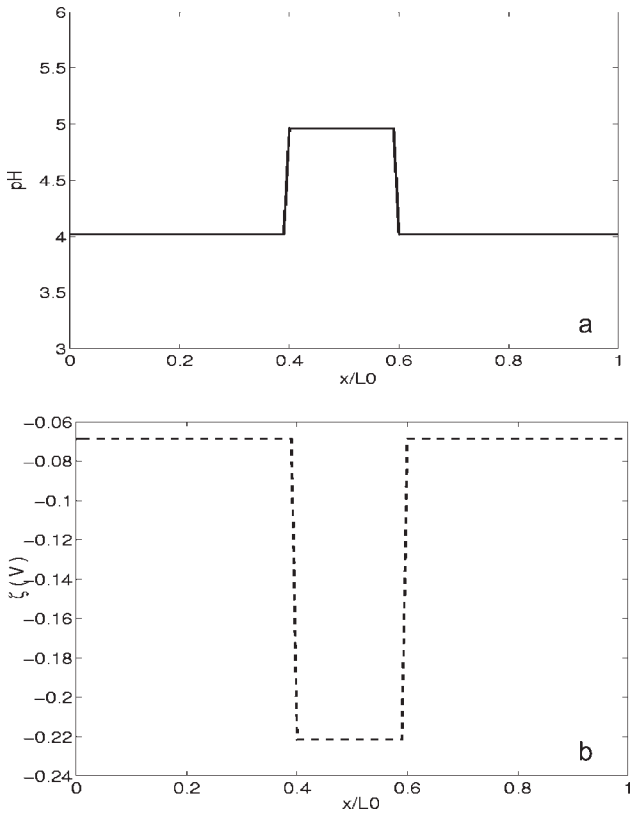

Figure 2. (a) Variation of the bottom wall pH with the axial position for the case in which the inlet buffer pH is 4.0, lengths of the transverse electrodes are $L_0/5$, and the electrodes are maintained at +15 V (top electrode) and +20 V (bottom electrode); (b) variation of the bottom wall zeta potential with the axial position for the case in which the inlet buffer pH is 4.0, lengths of the transverse electrodes are $L_0/5$, and the electrodes are maintained at +15 V (top electrode) and +20 V (bottom electrode).

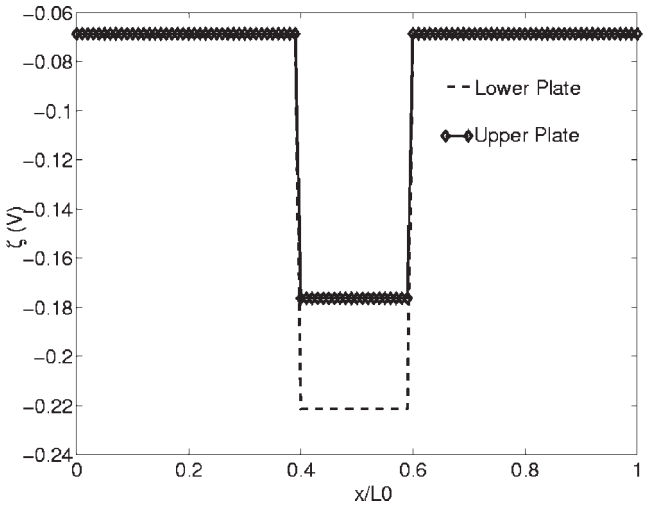

Figure 3. Variation of the wall zeta potential (ζ) with the axial position for the case in which the inlet buffer pH is 4.0, lengths of the transverse electrodes are $L_0/5$, and the electrodes are maintained at +15 V (top electrode) and +20 V (bottom electrode).

Here the upper plate is the top wall and the lower plate the bottom wall of the channel.

containing the transverse electrodes, the zeta potential at the bottom wall is observed to be more than that at the top wall, corresponding to the buffer-electrode arrangements employed in the present study. This leads to the development of a preferential excess charge density gradient that is directed from the top wall towards the bottom wall. The combination of this charge density gradient and the transverse electric field creates a transverse electro-osmotic body force, resulting in a transverse component of the electro-osmotic velocity being directed towards the bottom electrodes.

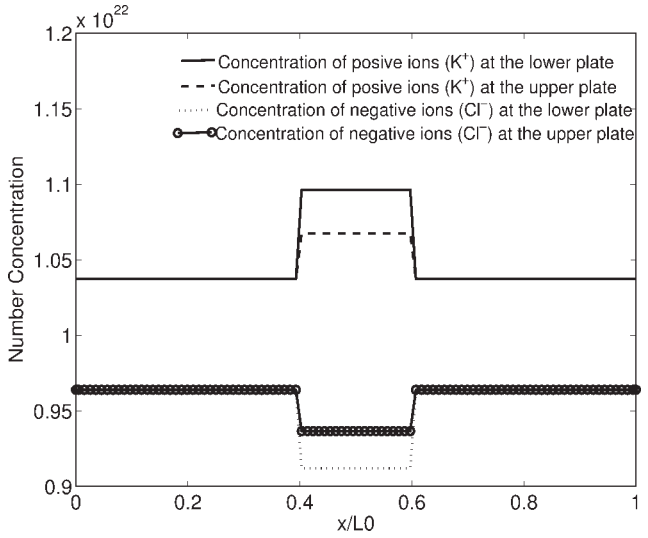

Figure 4. Variation of the ionic distribution for the positive (K^+) and negative ions (Cl^-) at the channel top and bottom walls with the axial position, for the case in which the inlet buffer pH is 4.0, lengths of the transverse electrodes are $L_0/5$, and the electrodes are maintained at +15 V (top electrode) and +20 V (bottom electrode).

Here the upper plate forms the top wall and the lower plate forms the bottom wall of the channel.

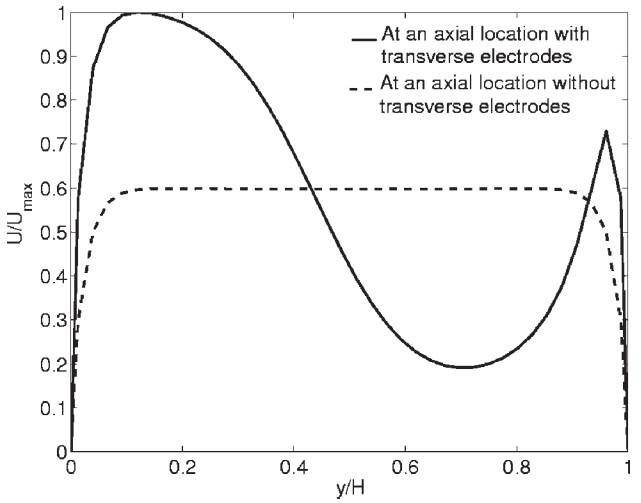

Figure 5. Comparison of the velocity profiles at different axial locations for the case in which the inlet buffer pH is 4.0, lengths of the transverse electrodes are $L_0/5$, and the electrodes are maintained at +15 V (top electrode) and +20 V (bottom electrode).

Effects on DNA hybridization

The present section discusses the influence of various electrical and flow parameters on the rate of DNA hybridization, consistent with the specific configuration employed in this study. The transverse velocity components being imparted by the cross-electrodes, indeed, play a pivotal role in dictating the rate of DNA hybridization in the microfluidic channel, as governed by the important system parameters. For illustrating this aspect, Figure 6 is plotted, which depicts the velocity fields within the microchannel, for an inlet buffer pH of 4.0, transverse electrode length of $L_0/5$, and the voltages of the top and the bottom electrodes as +15 V and +20 V, respectively. From Figure 6, it is evident that at sections upstream to the transverse electrodes, the velocity field is predominantly axial. On contrary, a significant transverse component (downward) velocity is imparted because of the effect of the presence of cross-electrodes in the further downstream sections. The net effect is an enhanced advective transport of the DNA molecules towards the bottom wall probe (Probe 2) that is located immediately downstream to the section containing the transverse electrodes. This ensures that despite the surface adsorption of the ssDNA molecules at the upstream probe location (Probe 1), considerable rates of migration of the ssDNA molecules from the buffer solution to the downstream probe location (Probe 2) can effectively be maintained. Thus, with the present configuration, the rate of DNA hybridization at the location of the Probe 2 is sub-

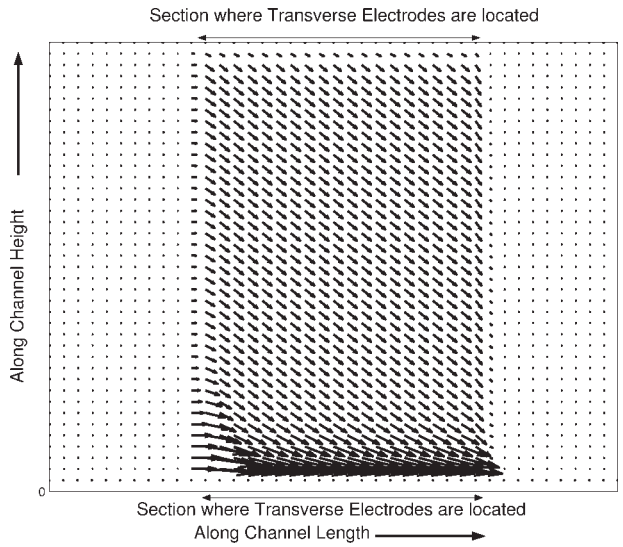

Figure 6. Velocity vectors at a specified portion of the flow domain that includes the transverse electrodes for the case in which the inlet buffer pH is 4.0, lengths of the transverse electrodes are $L_0/5$, and the electrodes are maintained at +15 V (top electrode) and +20 V (bottom electrode).

stantially enhanced, when compared with the case without transverse electrodes, as depicted in Figure 7.

To further elucidate the effects of various system parameters on the rate of DNA hybridization, as dictated by the mechanisms explained earlier, the influences of the following aspects are analyzed in further details, in the subsequent discussions:

(a). The pH of the inlet buffer
(b). The length of the transverse electrodes, and
(c). The voltages at which the top and the bottom electrodes are maintained.

Effect of variation of the pH of the inlet buffer. To exhibit the effect of variation of the inlet buffer pH on the rate of DNA hybridization at the capturing probes, we plot (Figure 8) the temporal variation of the concentration of the hybridized targets at both the probes, with variable pH values of the inlet buffer, all other conditions remaining unaltered. In general, it is observed that higher the inlet pH value, faster is the DNA hybridization rate, as apparent from Figure 8. This can be attributed to the fact that an increased value of the inlet buffer pH necessarily implies an increase in the wall pH, over and above the local pH augmentation effects induced by the transverse electrodes. This, in turn, leads to an enhancement in the effective zeta potential, thereby ensuring an augmented rate of convective transport of ss-DNA molecules, resulting in a improved DNA hybridization characteristics at both the capturing probes. However, the extent of enhancement in the rate of DNA hybridization, as achieved by using an inlet buffer of higher pH, is not identical for the two probes. It is critical to recognize in this respect that the negative y-gradient of the transverse components of the velocities near the cross-electrodes (due to the introduction of an additional vertically downward velocity component) also result in a positive x-gradient of the axial component of the flow velocity, so as to satisfy the continuity requirements (conservation of mass). As a consequence, an accelerated migration of the ssDNA molecules takes place towards the location of Probe 2. What follows from this argument is the fact that the enhancement effects in the rate of DNA hybridization, because of an augmented convective transport, are much more significant at the location of Probe 2, when compared with Probe 1. This relative enhancement

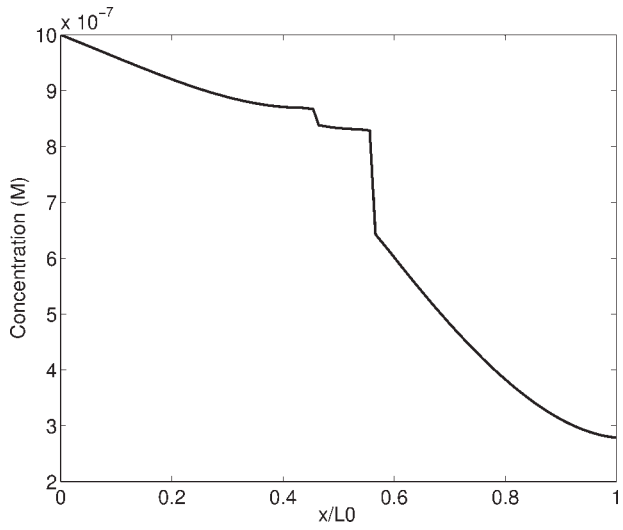

Figure 7. Variation of the film concentration with normalized axial coordinate for the case in which the inlet buffer pH is 4.0, lengths of the transverse electrodes are $L_0/5$, and the electrodes are maintained at +15 V (top electrode) and +20 V (bottom electrode).

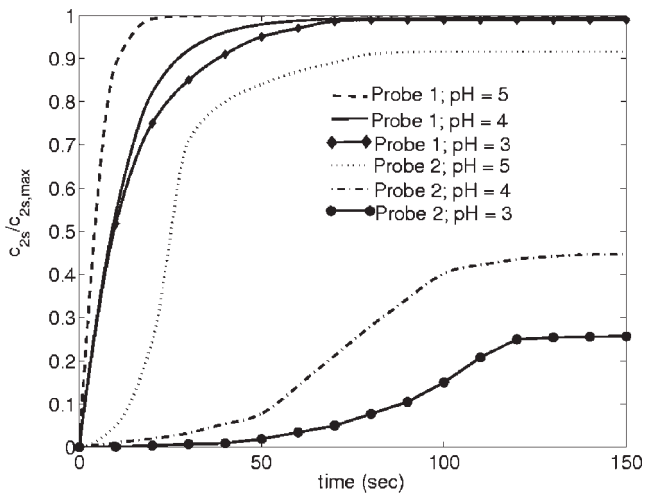

Figure 8. Temporal variation of the concentration of the hybridized targets at the two probe locations, for different inlet values of the buffer pH. Lengths of the transverse electrodes are $L_0/5$ and the electrodes are maintained at +15 V (top electrode) and +20 V (bottom electrode).

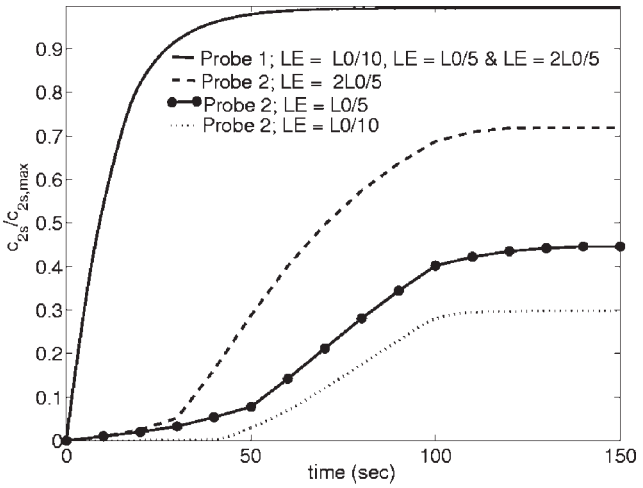

Figure 9. Temporal variation of the concentration of the hybridized targets at the two capturing probe locations, for different values of the transverse electrodes lengths.

The electrodes are maintained at +15 V (top electrode) and +20 V (bottom electrode), and the inlet buffer pH is taken to be 4.

is only possible because of the local increments in the magnitudes of the wall zeta potentials, on account of the transverse electrode effects.

Effect of the Variation of the Length of the Transverse Electrodes. To analyze the effects of variation of the length of the transverse electrodes on the rate of DNA hybridization at the probes, we plot Figure 9, which depicts the temporal variation of the concentration of the hybridized targets for different lengths of the transverse electrodes (i.e., different values of LE), keeping all other conditions unaltered. By altering the lengths of the transverse electrodes, the portion of the channel length over which the zeta potential is modified due to the 'field effect' is effectively varied. From Figure 9, it is evident that the rate of DNA hybridization at Probe 1, as indicated by the temporal variation of the concentration of the hybridized targets at that location, is insensitive to the changes in lengths of the transverse electrodes, because of the fact that the Probe 1 is located upstream relative to the transverse electrodes, and therefore carries no information of alteration of the wall zeta potential by virtue of their presence. At the location of Probe 2, however, influence of upstream transverse electrodes can be strongly felt. In general, it is revealed that longer the transverse electrodes, longer is the portion of the channel over which the 'field effect,' causing an enhanced localized axial transport and an effective 'push' towards the bottom wall leading to destruction of depletion layer, on account of enhanced zeta potential, is felt. The result is the improvement in the rate of DNA hybridization at Probe 2. However, it needs to be remembered at this point that the length of transverse electrodes cannot be indiscriminately increased so as to exploit a maximum advantage of the consequent augmentation in the rate of convective transport, mainly because of the technological constraints associated with the placement of the DNA probes devoid of any direct interference with the wall electrodes.

Effect of the Variation of the Voltages of the Transverse Electrodes. To exhibit the effect of the variation of voltages at the transverse electrodes on the rate of DNA hybridization, we plot Figure 10, which depicts the temporal variation of the concentration of the hybridized targets at the two probe locations, for different values of the transverse electrode voltages, all other conditions remaining unaltered. To demonstrate these aspects, following three cases are considered: (a) Case A: no transverse electrode, (b) Case B: +15V and +20V at the top and the bottom electrodes, respectively, (c) Case C: +15V and +65V at the top and the bottom electrodes, respectively. In each of three cases, the buffer pH is taken to be 4 and the transverse electrodes for Cases B and C are taken to be of length $L_0/5$. As expected, the hybridization pattern at Probe 1 is insensitive to the variations amongst the three different cases, since the Probe 1 is located upstream to the transverse electrodes. However, at the location of Probe 2, effects of voltages of the transverse electrodes are strongly felt. Higher the electrode potentials, more significant is the corresponding enhancement in the wall zeta potential, and stronger is the augmentation in the rate of electrokinetic convective transport and the effective downward 'push,' leading to a richer supply of DNA molecules to the downstream probe location (i.e., Probe 2), thereby ensuring improved hybridization rates. As a result, for higher values of the transverse electrode voltages, a nearly uniform rate of DNA hybridization can effectively be achieved at the different capturing probe locations, thereby virtually nullifying the counteracting effects of a continuous removal of the ss-DNA molecules from the bulk because of the specific and nonspecific hybridization effects at the fur-

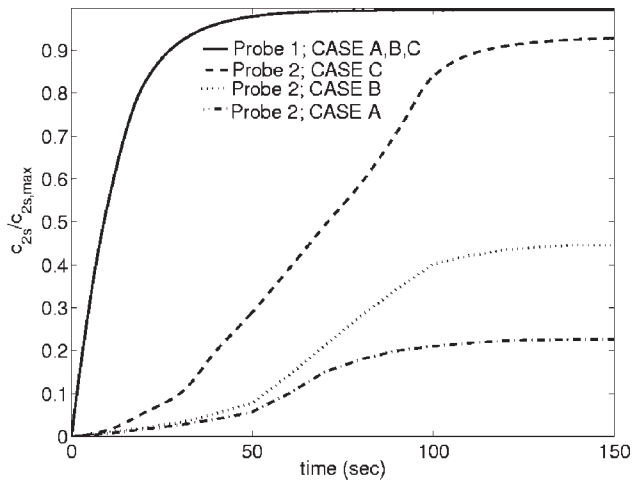

Figure 10. Temporal variation of the concentration of the hybridized targets at the two capturing probe locations, for the following cases, Case A: no transverse electrodes; Case B: the transverse electrodes are maintained at +20 V (the bottom electrode) and +15 V (top electrode); and Case C: the transverse electrodes are maintained at +65 V (the bottom electrode) and +15 V (top electrode).

Lengths of the transverse electrodes are $L_0/5$ and the inlet buffer pH is taken to be 4.

ther upstream sections. Such a uniform concentration distribution is often useful for the cases, in which one employs a single nucleic acid hybridization system, to accomplish multiple diagnostic purposes. However, it needs to be remembered here that the transverse electrode voltages cannot be incremented at will, in an effort to obtain the favorable effects mentioned as earlier. This is because of the fact that the resultant electric field needs to be constrained within stringent limits in practice, so as to ensure that the associated Joule heating effects are not strong enough to result in a denaturation of the thermally labile DNA samples. We present a critical assessment of this aspect in the subsequent subsection.

Other than the effects of these three significant operating parameters mentioned as earlier, it is important to recognize here that the channel height is also intuitively expected to bear significant consequences on the rate of DNA hybridization. However, it has already been demonstrated in the literature that the effect of the channel height on the rate of DNA hybridization becomes important[35] only if the transport is predominantly pressure-driven, since in such a case the velocity variations are strongly dependent on the transverse coordinates. On the other hand, for a pure electro-osmotic flow field, as considered in this study, the axial velocity components remain virtually uniform over the channel cross sections, provided that the channel dimensions are large enough (typically of the order of 1 μm or more) to ensure nonoverlapped EDL fields, so that the channel height does not play a critical role in influencing the rate of DNA hybridization under these conditions. However, in case of nanochannels, such effects can be of critical importance in determining the net rate of macromolecular transport and hybridization. For instance, in case of nanochannels, the net rate of macromolecular transport may be significantly reduced because of a hindered diffusive transport originated out of the confinement effects. Narrower the channel, stronger becomes this effect. However, since the present study is only confined to the electro-osmotically-driven DNA hybridization in microfluidic channels, analysis of the height-dependent macromolecular transport in nanochannels falls beyond the present scope, and accordingly, is not discussed here.

Limitations in Employing Transverse Electric Fields for Enhancing the Rate DNA Hybridization. 'Melting' or 'denaturation' of DNA is characterized by the separation of two DNA strands from an existing hybridized state. This splitting occurs at the melting temperature, T_m, defined as the temperature at which 50% of the oligonucleotides and their perfect complements are in duplex. To avoid problems like inappropriate duplex formation, primer mismatch etc., the hybridization is typically carried out $5^\circ - 10^\circ C$ below T_m. Hence it is important that the temperature rise due to Joule heating during hybridization is not more than around 5°C. This, in turn, imposes serious restraints to the upper limit of the electric field that can be employed to actuate the electrokinetic flows in the DNA hybridization assays. To assess this issue critically, it is imperative to obtain the temperature distributions along the channel bottom wall, for the Cases A, B, and C mentioned in the previous subsection, which are depicted in Figures 11a–c. For Case A (no transverse electrodes), the maximum temperature rise is found to be well within the permissible limits prescribed earlier, thereby avoiding any thermal denaturation of the hybridized

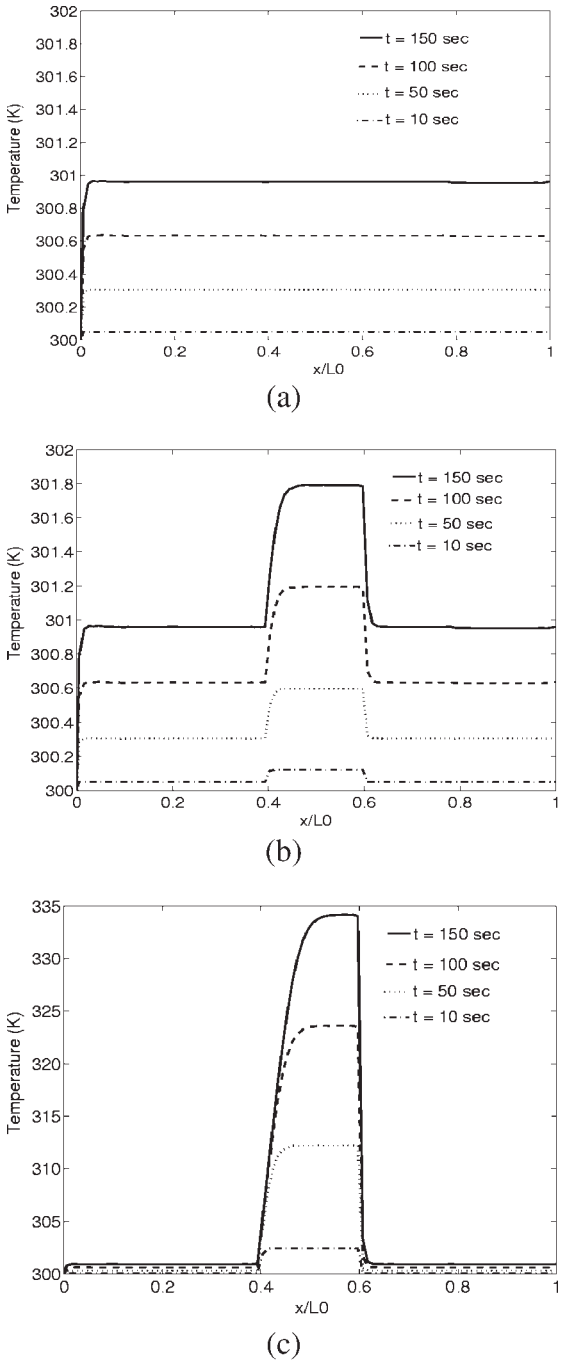

Figure 11. Temporal variation of temperature along the bottom wall of the channel in the axial direction, for (a) Case A, (b) Case B, and (c) Case C.

Detailed particulars of these three cases are mentioned in the caption of Figure 7.

DNA samples. So far as the Case B is concerned, it is revealed that the axial temperature profile along the bottom wall, at a given instant of time, exhibits the trend of an abrupt rise near the locations of placement of the transverse electrodes. However, for this case too, the maximum temperature rise at any portion of the channel wall is safely within the permissible limits to avoid DNA melting. Therefore, so

far as the DNA hybridization is concerned, the arrangement for Case B (with transverse electrodes) turns out to be more favorable than the same employed for Case A (without transverse electrodes). However, for Case C, it is found that the localized temperature rise on account of the placement of transverse electrodes turns out to be in the tune of 35°C (refer to Figure 11c), which is much above the safe permissible limit of about 5°C. This can be attributed to the existence of much stronger localized transverse potential gradients in Case C, when compared with that for the Cases A and B. For a physical assessment of the prevailing situation, a scaling argument in favor of such behaviour can be put forward, by noting that the maximum temperature rise, ΔT, can be estimated as

$$\Delta \mathrm{T} \sim \frac{\sigma(E_x^2 + E_y^2)\Delta t}{\rho C_\mathrm{p}} \tag{37}$$

where Δt is the time elapsed. In the earlier expression, $E_y \sim \frac{\Delta V_\mathrm{T}}{H}$, where ΔV_T is the potential difference between the transverse electrodes. Clearly, ΔV_T for Case C (i.e., 40 V) turns out to be much higher than that for Case B (i.e., 5 V), resulting in much greater temperature increments in the former case than the later. As a consequence, although the rate of DNA hybridization is clearly more favorable in Case C than in Case B, the former case does not offer with a technologically viable option for augmenting the hybridization performance in a DNA assay.

Conclusions

The present model discusses a novel approach to ensure a faster rate of DNA hybridization, by creating a localized pH gradient on employment of local transverse electric fields over selected portions of the channel length. Arrangement of such transverse electrodes is primarily motivated because of the following reason. A progressive depletion of the ss-DNA molecules from the bulk (owing to nonspecific adsorption and 3D hybridization at the probes that are located at further upstream sections), during their transport through the microchannel, is likely to result in a reduced rate of DNA hybridization at channel sections that are located further downstream. However, on employment of transverse electrode pairs, localized enhancements in the wall zeta potential can be achieved, which in turn, can promote a stronger convective transport, and accordingly, a faster rate of DNA hybridization can be achieved at capturing probes that are located further downstream relative to the channel inlet section. However, strength of the transverse electric field cannot be selected at will, but needs to be constrained within permissible limits, so as to ensure that no further thermal denaturation of the hybridized DNA molecules takes place. The present model provides with a scientific guideline for solution of the resultant optimization problem, so as to achieve the fastest rate of DNA hybridization without violating the upper limits of temperature rise that can be allowed in practice.

Literature Cited

1. Chan V, Graves DJ, McKenzie SE. The biophysics of DNA hybridization with immobilized oligonucleotide probes. *Biophys J*. 1995;69:2243–2255.
2. Axelrod D, Wang MD. Reduction-of-dimensionality kinetics at reaction-limited cell surface receptors. *Biophys J*. 1994;66:588–600.
3. Zeng J, Almadidy A, Watterson J, Krull UJ. Interfacial hybridization kinetics of oligonucleotides immobilized onto fused silica surfaces. *Sens Actuators B*. 2003;90:68–75.
4. Erickson D, Li D, Krull UJ. Modelling of DNA hybridization kinetics for spatially resolved biochips. *Anal Biochem.* 2003;317:186–200.
5. Das S, Das T, Chakraborty S. Modeling of coupled momentum, heat and solute Transport during DNA hybridization in a microchannel in presence of electro-osmotic effects and axial pressure gradients. *Microfluidics Nanofluidics*. 2006;2:37–49.
6. Hitt DL, McGarry M. Numerical simulations of laminar mixing surfaces in pulsatile microchannel flows. *Math Comput Simul*. 2004;65:399–416.
7. Glasgow I, Aubry N. Enhancement of microfluidic mixing using time pulsing. *Lab Chip*. 2003;3:114–120.
8. Glasgow I, Batton J, Aubry N. Electroosmotic mixing in microchannels. *Lab Chip*. 2004;4:558–562.
9. Liu RH, Stremler MA, Sharp KV, Olsen MG, Santiago JG, Adrian RJ, Aref H, Beebe DJ. Passive mixing in a three-dimensional serpentine microchannel. *J Microelectromech Syst*. 2000;9:190–207.
10. Xia HM, Wan SYM, Shu C, Chew YT. Chaotic micromixers using two-layer crossing channels to exhibit fast mixing at low Reynolds numbers. *Lab Chip*. 2005;5:748–755.
11. Johnson TJ, Ross D, Locascio LE. Rapid microfluidic mixing. *Anal Chem.* 2002;74:45–51.
12. Ajdari A. Generation of transverse fluid currents and forces by an electric field: electro-osmosis on charge-modulated and undulated surfaces. *Phy Rev E*. 1996;53:4996–5005.
13. Kuksenok O, Yeomans JM, Balazs AC. Using patterned substrates to promote mixing in microchannels. *Phys Rev E*. 2002;65:031502.
14. Zhang J, He G, Liu F. Electro-osmotic flow and mixing in heterogeneous microchannels. *Phys Rev E*. 2006;73:056305.
15. Tseng WL, Hsieh MM, Wang SJ, Chang HT. Effect of ionic strength, pH and polymer concentration on the separation of DNA fragments in the presence of electroosmotic flow. *J Chromatogr A*. 2000;894:219–230.
16. Peng XY, Li PCH. A three-dimensional flow control concept for single-cell experiments on a microchip. II. Fluorescein Diacetate metabolism and calcium mobilization in a single yeast cell as stimulated by glucose and pH changes. *Anal Chem*. 2004;76:5282–5292.
17. Righetti P, Bossi A. Isoelectric focusing of proteins and peptides in gel slabs and in capillaries. *Anal Chim Acta*. 1998;372:1–19.
18. Lee GB, Fu LM, Lee CY, Yang RJ. Dispersion control in microfluidic chips by localized ζ potential variation using the field effect. *Electrophoresis*. 2004;25:1879–1887.
19. Molloy RF, Leighton DT Jr. Binary oscillatory cross-flow electrophoresis: theory and experiments. *J Pharm Sci*. 1998;87:1270–1281.
20. Chen Z, Chauhan A. Taylor dispersion in cyclic electric field-flow fractionation. *Phys Fluid*. 2006;18:067105–067116.
21. Chen Z, Chauhan A. DNA separation by EFFF in a microchannel. *J Colloid Interface Science*. 2005;285:834–844.
22. Tang GY, Yang C, Chai JC, Gong HQ. Joule heating effect on electroosmotic flow and mass species transport in a microcapillary. *Int. J. Heat Mass Trans*. 2004;47:215–227.
23. Sonuart TL, Baygents JC. Electrically-driven fluid motion in channelswith streamwise gradients of the electrical conductivity. *Colloid Surf A*. 2001;195:59–75.
24. Dwyer JD, Bloomfield VA. Brownian dynamics simulation of probe diffusion in DNA: effects of probe size, charge and DNA concentration. *Biophys Chem*. 1995;57:55–64.
25. Phillies GDJ. Universal scaling equation for self-diffusion by macromolecules in solution. *Macromolecules*. 1986;19:2367–2376.
26. Tracy MA, Pecora R. Macromolecular synthesis, characterization and dynamics of a rod/sphere composite Liquid. *Macromolecules*. 1992;25:337–354.
27. Wattenbarger MR, Bloomfield VA, Bu Z, Russo P. Tracer diffusion of proteins in DNA solutions. *Macromolecules*. 1992;25:5263–5265.
28. Carré A, Lacarrière V, Birch W. Molecular interactions between DNA and an aminated glass substrate. *J Colloid Interface Sci*. 2003;260:49–55.

29. Parks GA. Isoelectric points of solid oxides solid hydroxides and aqueous hydroxo complex systems. *Chem Rev*. 1965;65:177–198.
30. Carré A, Roger F, Varinot C. Study of acid/base properties of oxide, oxide glass and glass-ceramic surfaces. *J Colloid Interface Sci*. 1992;154:174–183.
31. Kirby BJ, Hasselbrink EF. Jr. The ζ potential of microfluidic substrates. I. Theory, experimental techniques, and effects on separations. *Electrophoresis*. 2004;25:187–202.
32. Hayes MA, Ewing AG. Electroosmotic flow control and monitoring with an applied radial voltage for capillary zone electrophoresis. *Anal Chem*. 1992;64:512–516.
33. Lee CS, McManigill D, Wu CT, Patel B. Factors affecting direct control of electroosmosis using an external electric field in capillary electrophoresis. *Anal Chem*. 1991;63:1519–1523.
34. Wu HY, Liu CH. A novel electrokinetic micromixer. *Sens Actuators A*. 2005;118:107–115.
35. Kim JH, Marafie A, Jia X, Zoval JV, Madou M. Characterization of DNA hybridization kinetics in a microfluidic flow channel. *Sens Actuators B*. 2006;113:281–289.

Manuscript received July 6, 2006, and revision received Jan. 16, 2007.